ORIGINAL ARTICLE

Improving microstructural and mechanical properties of dissimilar friction stir welded AZ61/AZ40 joint

Liang Wang[1,2] · Jixiang Wang[3] · Chengwu Cui[3] · Peishan Zhou[2] · Bin Wang[2] · Hualin Zheng[1]

Abstract

This study focuses on the microstructure evolution and mechanical properties of dissimilar magnesium alloy friction stir welded AZ61/AZ40 joints achieved at different traverse speeds (50–130 mm/min) and a constant rotation speed (1200 rpm). The surfaces of the welds are relatively smooth without any obvious surface defects except for the FSW joint at a traverse speed of 50 mm/min. The nugget zone (NZ) is bowl-shaped due to the tapered probe. The Mg-based alloys were sufficiently mixed with each other in the NZ, and the interface was irregular. In addition, the NZ exhibits fine equiaxed grains due to dynamic recrystallization (DRX), and the grain size decreases with increasing traverse speed. The welded joints show a relatively discontinuous microhardness, and the lowest microhardness occurs in the thermo-mechanically affected zone (TMAZ) on the advancing side (AS). The strength increases as the traverse speed increases from 50 to 70 mm/min and then decreases as the traverse speed increases continually. An exceptionally high tensile strength of 235 MPa was achieved at a traverse speed of 70 mm/min. The combined effects of high-density dislocations and fine second phases (η-Al_8Mn_5 and β-$Mg_{17}Al_{12}$ phase) promote mechanical properties.

Keywords Friction stir welding · Dissimilar magnesium alloy · Traverse speed · Microstructure · Mechanical properties

1 Introduction

Magnesium (Mg) alloys are ideal for the automotive and aerospace industries because they exhibit light weight [1], high specific strength [2], and machining performance [3]. Choosing lightweight alloys, Mg alloys and high-strength materials can effectively reduce vehicle weight and achieve a win−win situation of safety and environmental protection. Establishing a reliable joining process can widen the applications of Mg alloys [4]. Studying and optimizing the welding performance of Mg alloys lightweight structural components can be used to improve the mechanical properties of Mg alloys and expand their application fields. However, due to the high thermal conductivity and low melting point of Mg alloys, the traditional fusion welding of Mg alloy joints faces many challenges, such as grain coarsening [2], heat affected zone (HAZ) widening [5], intolerable distortions [6], hot cracks [7] and evaporative loss of alloying elements, which restrict the applications of Mg alloy welding structures. Therefore, in response to the shortcomings of traditional fusion welding of magnesium alloys, it is necessary to conduct systematic research on new methods of Mg alloy welding. Friction stir welding (FSW) is the most promising development in the field of Mg alloy joining in recent years and can significantly avoid the above issues [8].

At present, FSW has been successfully used to join a variety of Mg alloys, such as ZK60 [6], ZK61 [9], AM60/AZ31 [10], AM50/AZ31 [11], AZ31 [12], and other series of Mg alloys. It is well known that a reliable welded joint has a positive correlation with the heat input and thermoplastic deformation, which is related to the FSW parameters (such as the rotation speed, traverse speed, and size of the stirring tool), in particular, the ratio of the rotation speed to the traverse speed (denoted as ω/ν) [13]. With respect to the mechanical properties, the welding temperature of FSW is much lower

✉ Bin Wang
liangw1989@163.com

✉ Hualin Zheng
13709038896@163.com

1 School of Mechatronic Engineering, Southwest Petroleum University, Chengdu 610500, China

2 School of New Energy and Materials, Southwest Petroleum University, Chengdu 610500, China

3 China Petroleum Pipeline Institute Co., Ltd, Langfang 065000, China

than that of the traditional fusion welding process. In general, the temperature under stirring heat ranges from 300 ℃ to 470 ℃, which is significantly affected by the ratio of ω/ν. The heat input unit length decreases with the traverse speed, and the grain size also decreases. However, the influence of FSW parameters on joint quality is diverse. Yang et al. [14] studied the microstructure and mechanical properties of friction stir welded joints of 6 mm thick extruded AZ80 Mg alloy. They found that the grain size of the nugget zone (NZ) increases as the traverse speed increases, and a uniform microstructure is formed in the joint at a low traverse speed. During FSW, dynamic recrystallization (DRX) usually occurs in the NZ of the welded joint and causes microstructure refinement to greatly improve the mechanical properties. In general, DRX can be divided into three main mechanisms in Mg alloys, i.e., discontinuous dynamic recrystallization (DDRX), continuous dynamic recrystallization (CDRX), and twin dynamic recrystallization (TDRX) [15]. Lee et al. [16] studied the FSW of dissimilar Mg alloys AZ31 and AZ91 with a thickness of 4 mm and indicated that DRX and grain growth occur in the NZ, which is mainly composed of AZ31 Mg alloy placed on the RS.

For the dissimilar friction stir welded joint, the resultant grain structure in the weld determines the properties of the welded joint, and the abnormal microstructure severely affects the welded joint quality. In addition, the properties also mainly depend on mechanical interlocking (tortuous bonding interface) and metallurgical bonding (intermetallic compounds (IMCs)) [8]. Liu et al. [17] studied the effect of FSW parameters (rotation speed and traverse speed) on the material arrangement and mechanical properties of AZ80/AZ31 dissimilar Mg alloy FSW joints. Sunil et al. [18] found fine grains and the second phase of β-$Mg_{17}Al_{12}$ in the NZ of AZ31/AZ91 Mg alloy dissimilar FSW joints, which have a clear bonding interface between the NZ and TMAZ. The second phase in the NZ results in an increase in microhardness. Liu et al. [19] reported that the base metal (BM) mixing, grain refinement, and decomposition of the second phase of the ZK60/AZ31 dissimilar Mg alloy welded joint result in a significant increase in the microhardness of the NZ compared to the two BMs. Yang et al. [14] found that the coarse β-$Mg_{17}Al_{12}$ phase dissolved during FSW, and only a small amount of the β phase in the NZ. Luo et al. [20] studied the microstructure evolution and mechanical properties of friction stir welded joints of Mg–Zn–Gd and Mg–Al–Zn dissimilar Mg alloys (ZG61/AZ91D), and severe deformation and material flow occurred in the NZ at high strain rates and temperatures. There is no obvious joining interface or IMCs at the interface of the two Mg alloys, forming the Mg_3Zn_6Gd phase due to mutual diffusion between Zn and Al alloying elements. Templeman et al. [11] investigated the FSW joint of AM50/AZ31 Mg alloys and found that the dislocation rearrangement in AM50 is a subgrain boundary, indicating CDRX. The AZ31

magnesium alloy undergoes grain boundary movement and twin rotation relative to the matrix, transforming into low-angle grain boundaries, indicating DDRX. The dissolution of the rich Al phase β-$Mg_{17}Al_{12}$ leads to an increase in the Al content in the matrix of the NZ, resulting in the NZ exhibiting a higher potential than the BMs.

In general, the tensile properties of the FSW welded joint were lower than those of the BMs, which was mainly attributed to the severe strain localization in the joints [21]. Moreover, the fracture locations might occur in different regions and shift in the FSW welded joint. Huetsch et al. [22] studied the local stress of AZ31 Mg alloy after FSW, indicating that the uneven local stress results in the final fracture occurring in the thermos-mechanically affected zone (TMAZ) on the retreating side (RS). Shang et al. [23] also pointed out that the crack shift is mainly attributed to the strain localization, which is generated by the incompatible deformation of different subregions. The twinning at the edge of the nugget zone and the slip near the edge of the nugget zone led to uneven deformation in this area. The microstructure and the texture evolution in both the NZ and TMAZ played an important role in the nonuniform deformation behavior [24] in view of the topic phenomena of dissimilar Mg alloys FSW, which is different from single Mg alloys FSW, including material flow, texture evolution, material location and their effects on the mechanical properties. Considering the uniqueness of each series and grade of Mg alloy, different grades of magnesium alloy welding will have different characteristics.

In this study, AZ61A and AZ40M are two common commercial Mg alloys in the automotive and aerospace industries selected as the base metals (BMs). AZ40M has better corrosion resistance, and AZ61A has better plastic formability and impact resistance. Therefore, the dissimilar AZ61A/AZ40M Mg alloy FSW joint can meet the requirements of Mg alloys in different working environments. However, there is still a lack of relevant studies on dissimilar AZ61A/AZ40M Mg alloy FSW process parameters. Hence, the microstructure and mechanical properties of dissimilar AZ61/AZ40 Mg alloy FSW joints at different traverse speeds and significantly high strength joints were obtained. Moreover, the reason for the dissimilar friction stir welded AZ61/AZ40 joint fracture behavior was analyzed in this study.

2 Materials and experimental procedures

The Mg alloys used in this study were AZ40M and AZ61A Mg alloy plates with dimensions of $200 \times 100 \times 6.2$ mm^3 welded by FSW. The chemical compositions of the base metal are shown in Table 1. The microstructure of the BMs is shown in Fig. 1, and the grains of the two base metals are

Table 1 The chemical compositions of AZ40M and AZ61A alloy (wt%)

Alloy	Si	Cu	Fe	Ni	Al	Mn	Zn	Mg
AZ61A	≤0.08	≤0.01	≤0.003	≤0.001	5.9	0.38	0.89	Bal
AZ40M	0.026	0.002	0.0023	0.00047	3.6	0.29	0.47	Bal
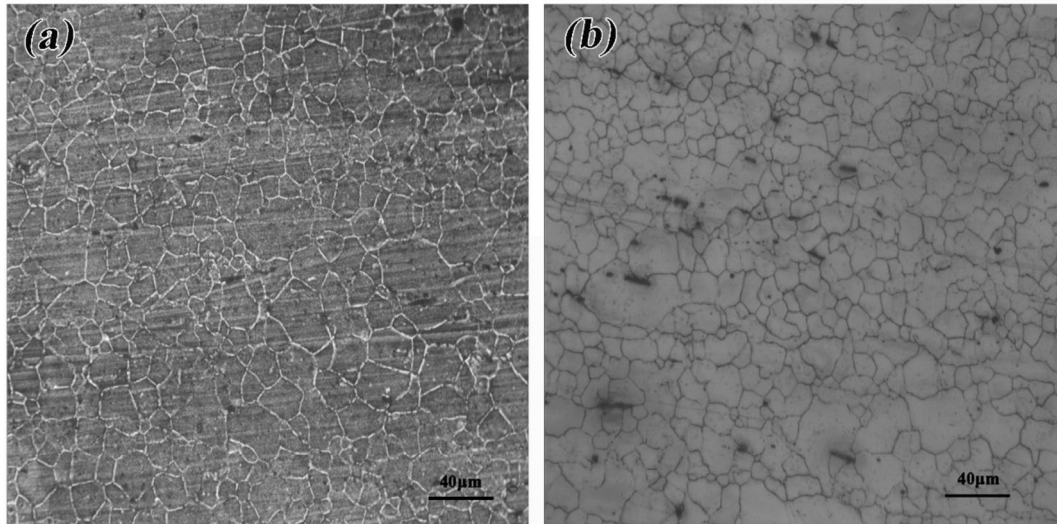
Fig. 1 The microstructure of the BMs, **a** AZ40M; **b** AZ61A

Table 2 The mechanical properties of the AZ40M and AZ61A alloy

Alloy	Yield strength/MPa	Ultimate tensile strength/MPa	Elongation/%
AZ61A	104.7 ± 8.3	315.6 ± 7.4	27.8 ± 3.4
AZ40M	106.3 ± 11.6	295.4 ± 19.6	18.2 ± 2.6

relatively coarse. The grain size distribution of the AZ40M Mg alloy is relatively uniform to that of the AZ61A Mg alloy. Some large grains are distributed among the refined equiaxed grains, and Zhang et al. [25] indicated that a bimodal/multimodal microstructure is beneficial for improving the ductility of Mg alloys. The mechanical properties of the AZ40M and AZ61A alloys are shown in Table 2. The yield strength of AZ40M is close to that of AZ61A, and the ultimate tensile strength and elongation of AZ40M are higher than those of AZ61A; thus, AZ40M was placed on the advancing side (AS).

The friction stir welding experiment was carried out using an FSW-058 friction stir welding machine. The shaft shoulder of the stirring head is a concave threaded shaft shoulder, and the diameter of the shaft shoulder is 15 mm; the length of the stirring probe is 5.9 mm, the bottom diameter is 6.4 mm, and the end diameter is 4 mm, as shown in Fig. 2. Before FSW, the surface of the plates was polished with SiC abrasive papers and acetone in sequence to remove oil stain and oxide layers. In this study, the welds were manufactured at traverse speeds of 50, 70, 90, 110, and 130 mm/min. The constant rotational speed was 1200 rpm, and the tool tilt was 3° with a downwards shaft shoulder of 0.3 mm.

After FSW, metallographic samples were cut vertically to the welding direction of FSW to investigate the microstructure characteristics. Standard grinding and polishing techniques were employed to obtain the mirror surface. The polished surface was etched with a solution of 8% nitric acid aqueous solution and 5% oxalic acid aqueous solution to reveal the flow patterns and microstructures via a DMIE200M optical microscope (OM). A Zeiss EV018 scanning electron microscope (SEM) (with EDS) was used to study the precipitation phase of the FSW joints. Transmission electron microscopy (TEM) foils were cut from the samples and mechanically ground to approximately 50 μm thickness. Disks (3 mm) were punched from the foils and twin-jet electropolished with a solution of 10% perchloric acid + 90% absolute ethanol as the electrolyte at −30 ℃. Foils were examined with an FEI Tecnai G2 F20 TEM operated at 200 kV.

The microhardness of the specimens was measured on an HVD-2000TM/LCD pyramidal indenter with a test load of $100 \times g$ for 10 s. The hardness of the specimens was measured along the mid-thickness of the joints' cross section, and the testing points included the base metal (BM), heat affected zone (HAZ), thermomechanical affected zone
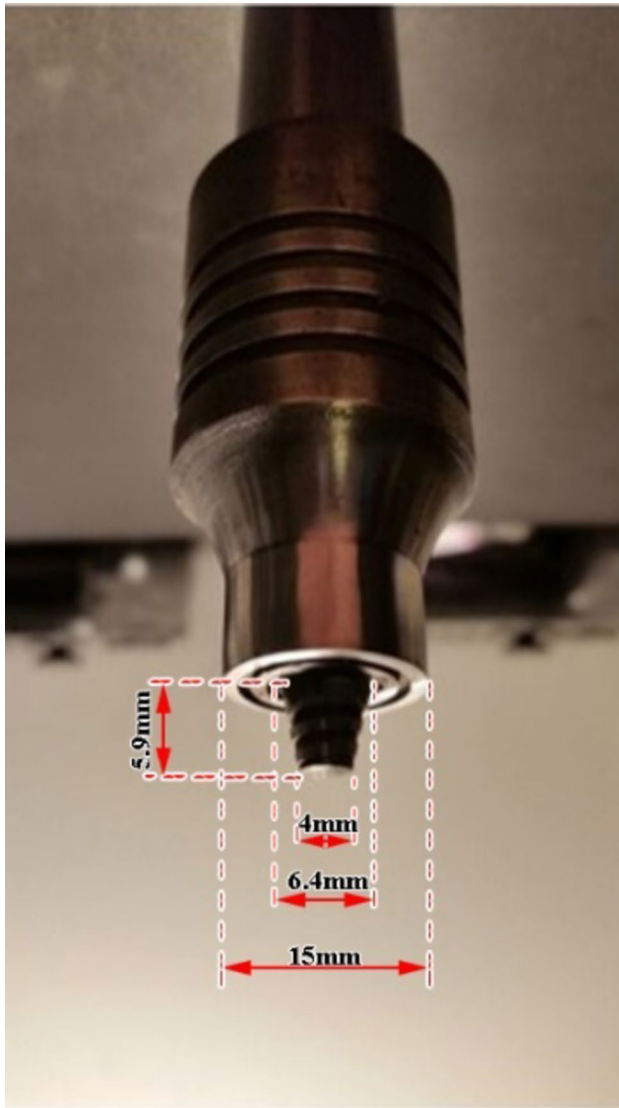
Fig. 2 The shape and size of the friction stir welding tool

(TMAZ), and nugget zone (NZ). The tensile specimens were cut vertically to the welding direction of the FSW joints. The tensile specimens with a width of 25 mm and a gage length of 76 mm were machined according to the ASTM E8M specification, and the tensile tests were carried out on the SHT 4605 testing machine at room temperature with a low strain rate of 5×10^{-4} s^{-1}. Three parallel tensile specimens were prepared for the tensile tests, and the average value was used as the result.

3 Results and discussion

3.1 Macrostructure characterization

The surface morphologies of FSW joints obtained with different process parameters are shown in Fig. 3. The surfaces of the welds are relatively smooth without any obvious surface defects except for the FSW joint at a traverse speed of 50 mm/min (Fig. 3a). From Fig. 3a, there is a crack with a length of approximately 50 mm observed in the initial stage of welding. This might be due to the relatively high heat input when the traverse speed was 50 mm/min and the rotational speed was 1200 rpm. The Mg alloys liquefied and formed cracks during the solidification process. In general, there is a difference in heat input in a single-pass friction stir welded joint, i.e., the heat input in the stable and end stages of the weld is higher than that in the initial stage [26]. The formation of this surface crack is not conducive to the mechanical properties of the joint. Moreover, small flash and little arc corrugation are clear on the weld surfaces produced at high traverse speeds of 70 ~ 130 mm/min. In addition, the flash and arc corrugation on the weld surfaces is eliminated when the traverse speed is greater than 110 mm/min, especially flash, as shown in Fig. 4d and e. According to Fig. 4,
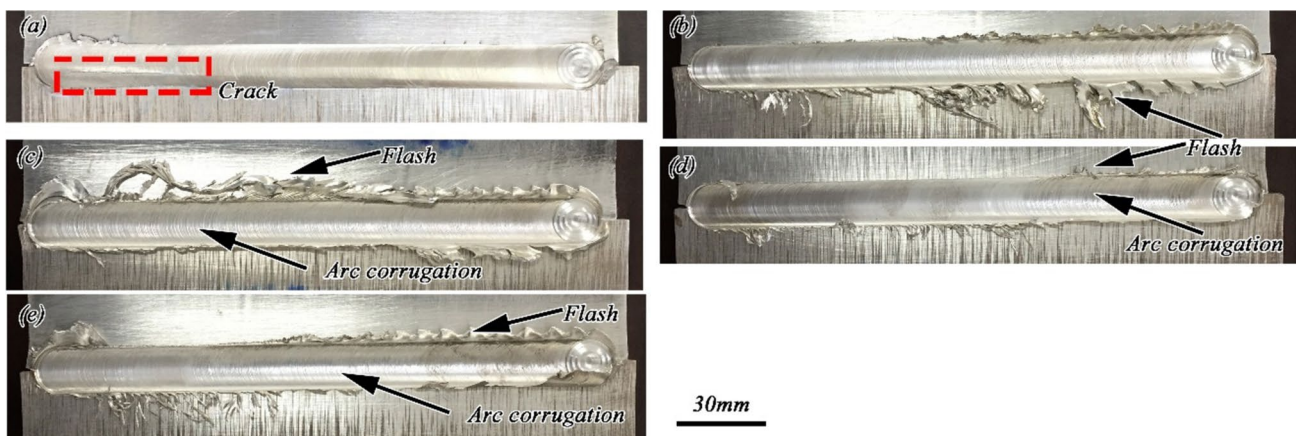

Fig. 3 The surfaces of the FSW joints at various traverse speeds **a** 50 mm/min; **b** 70 mm/min; **c** 90 mm/min; **d** 110 mm/min and **e** 130 mm/min

with the increase in traverse speed, the surface flash of the FSW joint gradually decreases.

The cross-sectional macrographs of the FSW joints at various traverse speeds are shown in Fig. 4. It is clear that relatively symmetric joints throughout the thickness were obtained at all traverse speeds. The FSW joints consist of the NZ, TMAZ, HAZ, and BM. During the FSW process, microstructure evolution and weld formation are generally affected by the shape of the probe, which will directly affect the heat input and material flow [27]. Therefore, all joints show the typically basin-shaped NZ due to the tapered probe. In addition, all specimens have sound joints except the specimen at a traverse speed of 50 mm/min, as shown in Fig. 4a. There are obvious tunnel and void-type defects in the NZ of the FSW joint, and the onion ring morphology is only visible at the root weld (Fig. 4a). The defects disappeared when the traverse speed was greater than 70 mm/min. This might be because the joint obtained under the process parameters of 1200 rpm–50 mm/min had insufficient heat input, which in turn affected the material flow and finally formed a tunnel in the NZ of the weld. In general, the slowing traverse speed might cause a higher heat input. However, it should be noted that when the temperature in the weld reaches a certain level, the friction coefficient of the material will decrease, so the heat input in the weld will not increase with increasing rotation speed or decreasing welding speed. In addition, when the heat in and out of the weld seam is too high, the plasticized metal will adhere too much to the inner surface of the stirring head shoulder, reducing the plasticized volume of the material.

The Mg alloys on both sides formed a relatively sufficient material mixing with each other in the NZ, and the interface was irregular. An obvious onion ring shape can be observed in the middle and bottom of the NZ, as shown in Fig. 4b-e. In addition, due to the material flow in the thickness direction of the plate, Mg alloys can be observed in the middle and bottom of the NZ corresponding to the threads on the tapered threaded pins. The material at the top of the joint is in direct contact with the shoulder, and the heat input and the temperature obtained by it are relatively high. During the FSW process, the material flow at the top of the joint is mainly driven by the rotation of the shoulder, which obtains a relatively high heat input and temperature. Moreover, the material flow at the top of the joint is mainly driven by the rotation of the shoulder, and in the middle of the NZ, it is mainly driven by the stirring probe, in which the temperature is lower than that of the top.

3.2 Materials flow

To reveal the materials flow during the FSW process, Fig. 5 shows the material flow patterns at the transverse cross section of the FSW joint at a traverse speed of 70 mm/min. In addition, the interface between AZ40M and AZ61A in the NZ can also be visibly identified because of the discrepancy in corrosion resistance. The dark area is RS-AZ61A, and the gray area is AS-AZ40M. The upper part of the FSW joint shows horizontal flow, as shown in Fig. 5a, b, c. The other parts show obvious U-shaped flow traces, as indicated by the red arrows in Fig. 5. The materials are stirred into the
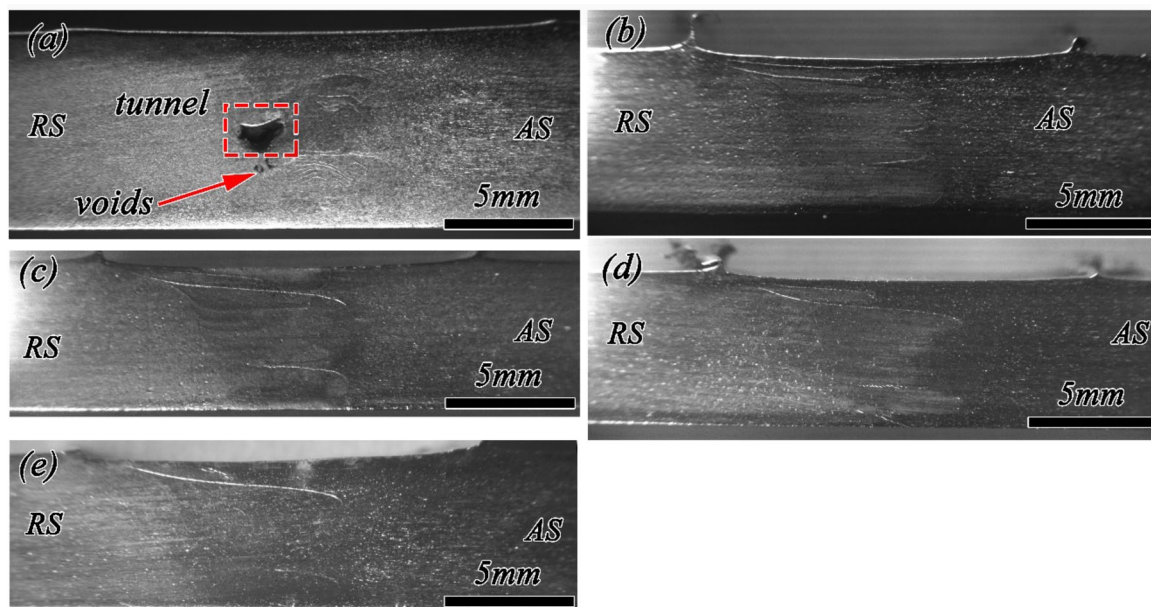

Fig. 4 Macrostructure of the FSW joints at various traverse speeds **a** 50 mm/min; **b** 70 mm/min; **c** 90 mm/min; **d** 110 mm/min and **e** 130 mm/min
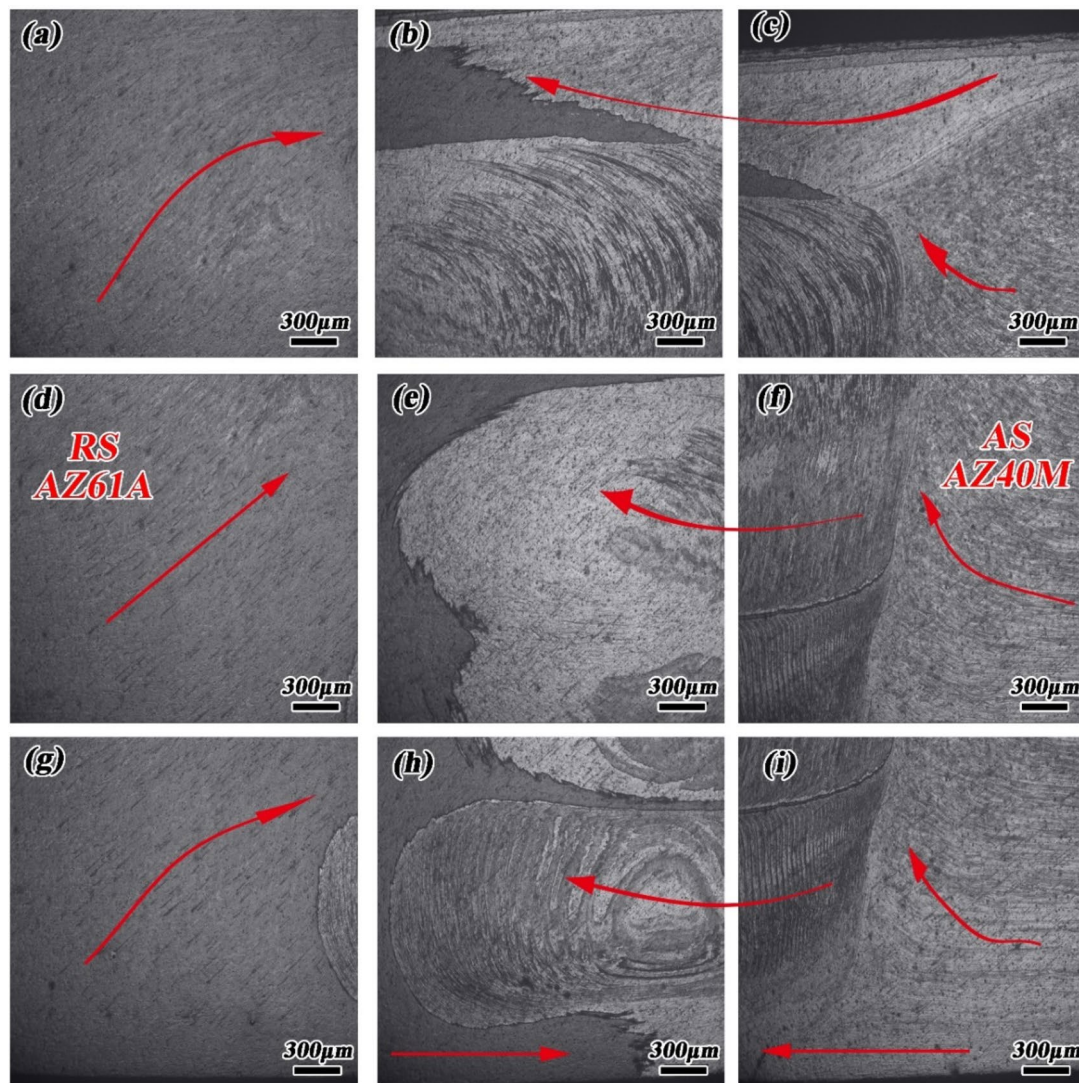
Fig. 5 OM images at the cross section of the welded joint at the traverse speed of 70 mm/min **a** top of RS-TMAZ, **b** top of NZ, **c** top of AS-TMAZ, **d** middle of RS-TMAZ, **e** middle of NZ, **f** middle of AS-TMAZ, **g** bottom of RS-TMAZ, **h** bottom of NZ, **i** bottom of AS-TMAZ

bottom due to the drive force of the stirring shoulder and pushed upwards by the right-hand pin thread [24]. Figure 5b, e, h shows the NZ of the FSW joint, and the "onion ring" is obvious, indicating that the two BMs were inter-locked with each other.

A cross-sectional macrostructure of the FSW joint is obtained at a traverse speed of 70 mm/min in Fig. 6. From Fig. 6a, the two different BMs interlock into each other, and it is obvious that the materials flow and several deformations take place because of the high rotation speed and strain rate. In addition, under the effect of the stirring tool, AZ40M stretches into deformation banded structures. The interface between AZ61A and AZ40M seems to be an "onion ring", which has been studied widely in previous papers [28]. From Fig. 6b, it can be seen that there is no significant IMC layer at the interface, which exhibits a tortuous shape due to the

combined effects of the heat input and high mechanical force during FSW. In addition, the distribution of three main elements (Mg, Al and Zn) at the interface of the two BMs is also shown in Fig. 6b. There is a smooth change in the content of the main elements at the interface. According to the chemical components of the BMs, Al and Zn diffuse from AZ61A to AZ40M.

3.3 Microstructure evolution

The microstructure of the NZ of the joints with different traverse speeds from 50 to 130 mm/min is shown in Fig. 7. The NZ experienced dynamic recrystallization (DRX) due to the combined effects of the welding heat input and the mechanical stirring of the stirring tool, and the microstructures all show fine equiaxed grains. In general, the grain
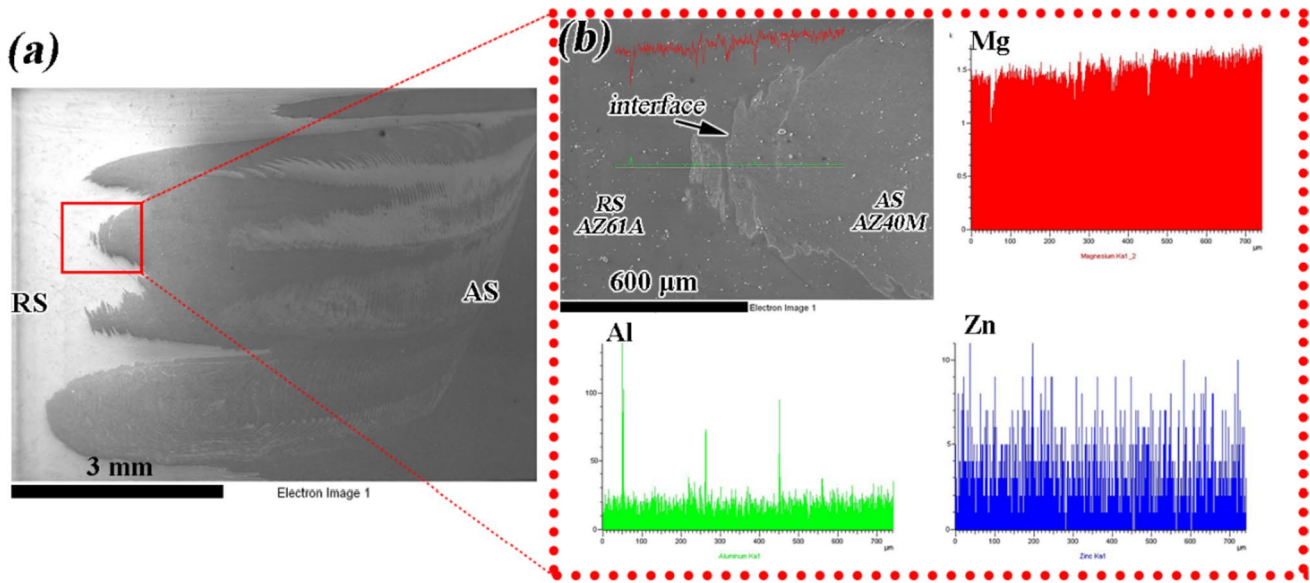
Fig. 6 Interface of the two BMs in FSW joint obtained at the traverse speed of 70 mm/min

size is significantly affected by the ratio of rotation rate to traverse speed (denoted as ω/ν) due to different degrees of heat input and thermoplastic deformation. Therefore, Fig. 7a shows the coarsest grains with an average grain size of 15.5 μm at a high ω/ν ratio with a traverse speed of 50 mm/min. With an increasing traverse speed, the grain size of the specimen with a traverse speed of 130 mm/min decreases to 12.5 μm. As the welding speed increases, the microstructure in the middle of the weld nugget area decreases, but defects, such as flash and holes increase.

Figure 8 shows the XRD results of the BMs and experimental welded joints. It is clear that the BMs were composed
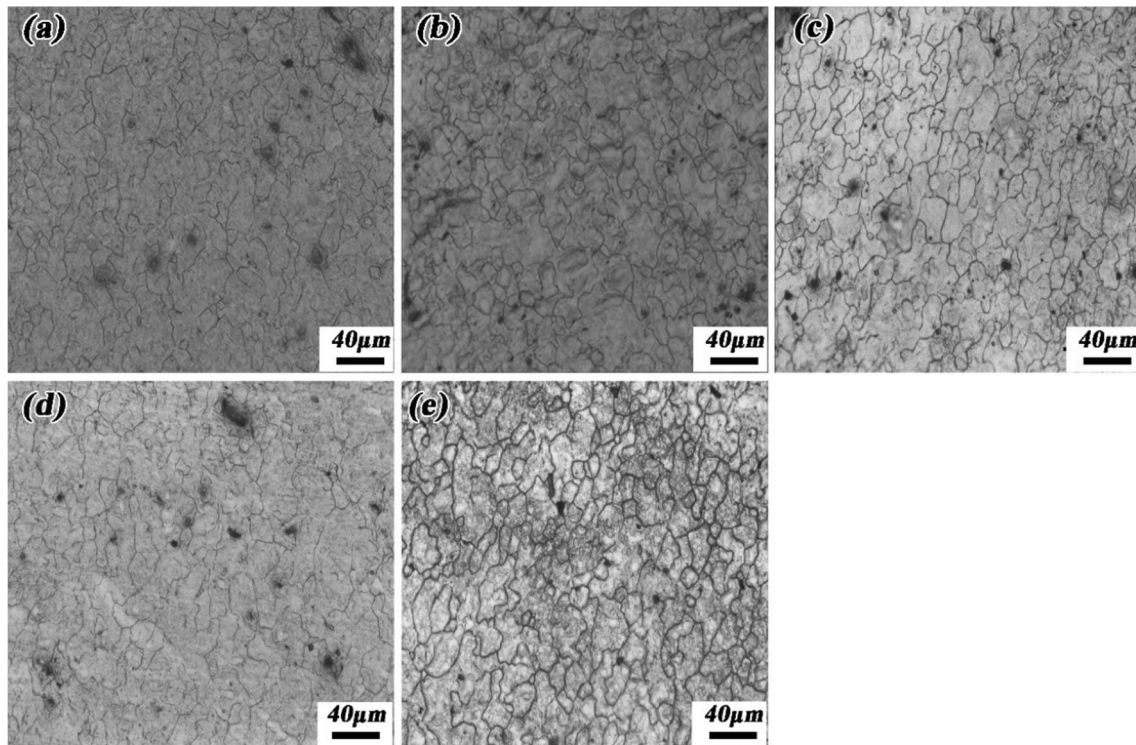

Fig. 7 Microstructure of the NZ at various rotational speeds **a** 50 mm/min; **b** 70 mm/min; **c** 90 mm/min; **d** 110 mm/min and **e** 130 mm/min

of α-Mg, β-Mg$_{17}$Al$_{12}$ and η-Al$_8$Mn$_5$ phases. After FSW, the welded joints were composed of the same phases. To further investigate the effect of the traverse speed on the second-phase particles, SEM−EDS and TEM were performed.
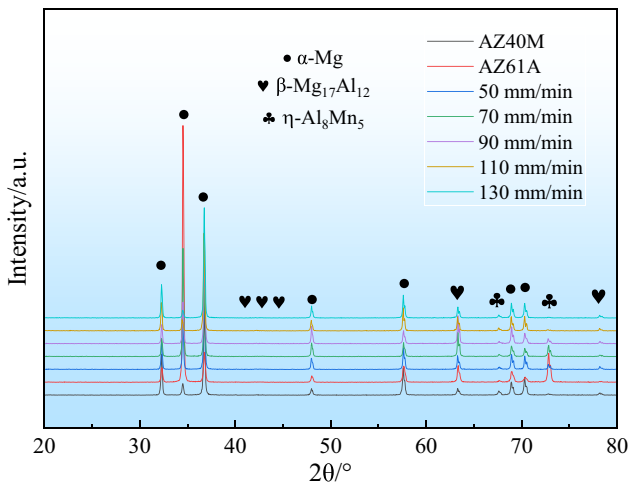

Fig. 8 XRD results of experimental welded joints

The second phases of the NZ with rotational speeds of 70 mm/min and 130 mm/min were analyzed by SEM and EDS, as shown in Fig. 9. The second phase particles in the NZ were fine and distributed uniformly, and the sizes of the particles in both joints were similar. Generally, as hard and brittle particles, the second phases in the BMs were extruded and rotating sheared by the stirring tool first during the process of friction stir welding. Then, the second phases were broken down and turned into fine particles. Therefore, it can be seen that the NZ is mainly composed of uniformly distributed small precipitates, as shown in Fig. 9a and b. Theoretically, the fine and evenly distributed second phases can increase the strength of joints [10]. The corresponding EDS results show that the second phase in the NZ is mainly composed of Al, Mg, and Mn, which is mainly the Mg-Al-Mn rich phase. This is consistent with the XRD results.

Figure 10 shows the second phases and dislocations in the NZ of the welded joint at a traverse speed of 70 mm/min. In Fig. 10a, the typical elliptical and rod-shaped precipitates are β-Mg$_{17}$Al$_{12}$ and η-Al$_8$Mn$_5$, respectively. Figure 10b, c shows that high-density dislocations piled up the grain boundaries. The intragranular dislocation movement was
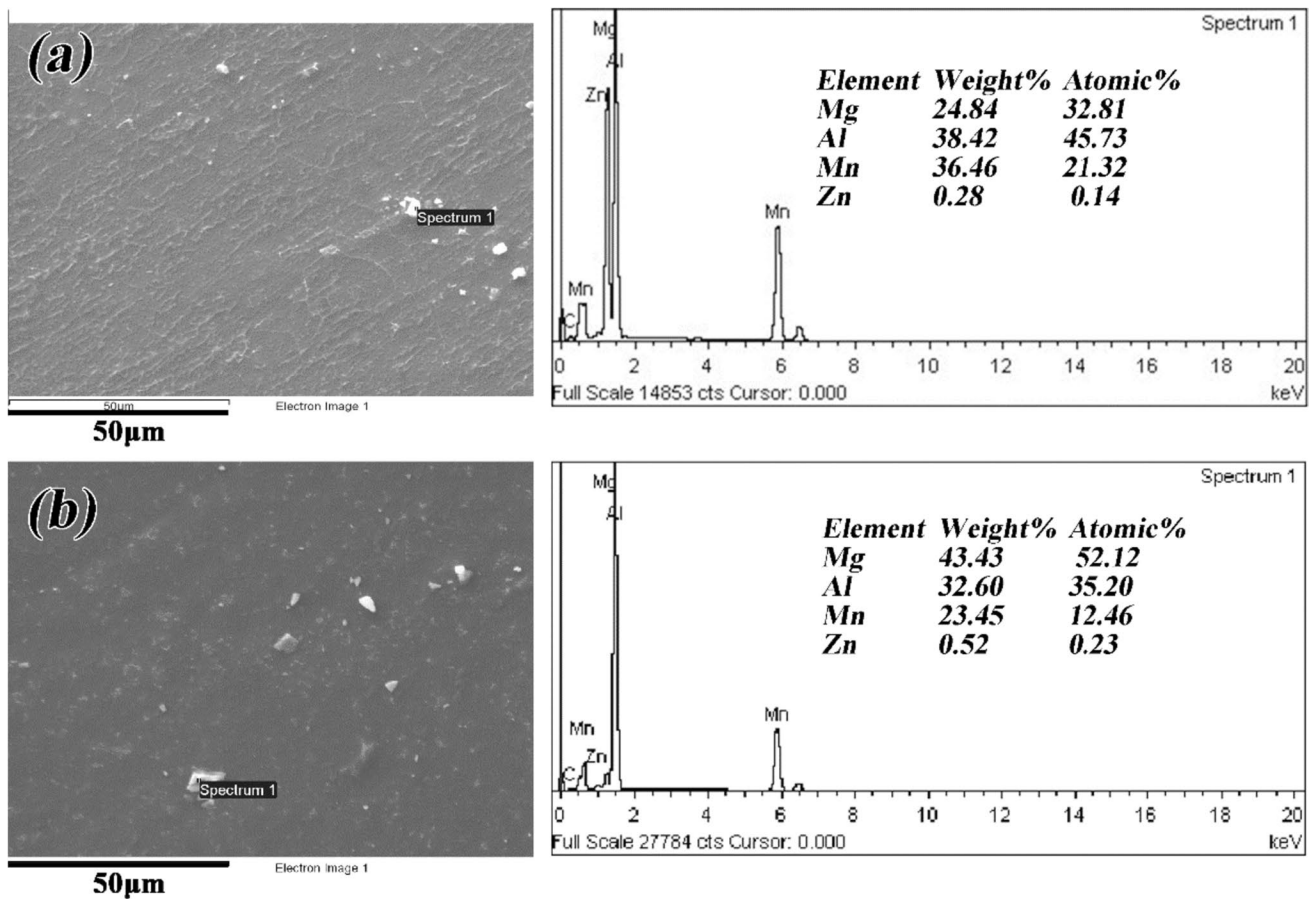

Fig. 9 SEM images showing second phases in the experimental welded joint **a** 70 mm/min; **b** 130 mm/min

hindered by the grain boundaries, resulting in the accumulation of high-density dislocations at the grain boundaries. From Fig. 10d, the interaction between high-density dislocations and β-Mg$_{17}$Al$_{12}$ precipitates at the grain boundaries in the NZ can improve the mechanical properties.

3.4 Microhardness

Figure 11 shows the microhardness of the experimental welded joints with different traverse speeds from 70 mm/min to 130 mm/min. The microhardness value was measured in the middle of the thickness with 1 mm intervals. The microhardness value of the welded zone has a relatively large variation compared to that of the BMs. The microhardness values vary between 50.4 HV to 69.4 HV. The average microhardness values in the NZ of all welded joints are 61.7, 54.4, 57.1, 62.0, and 61.2 HV for traverse speeds of 50, 70, 90, 110, and 130 mm/min, respectively. The microhardness distribution shows a relatively obvious discontinuity between the NZ and HAZ + TMAZ in each process parameter. It should be noted that the microhardness affected by the grain size does not follow the Hall−Petch equation. In this
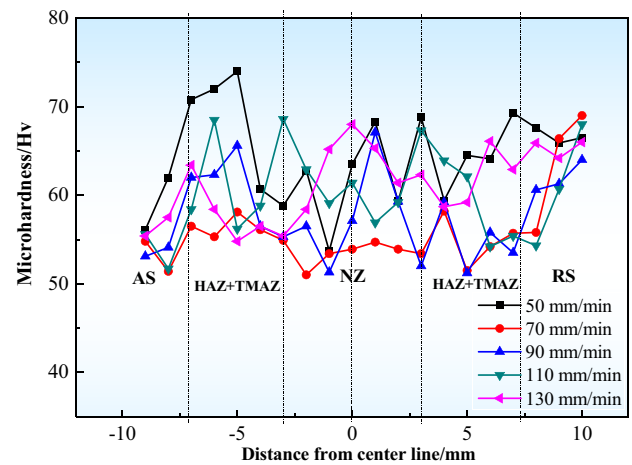
Fig. 11 Microhardness distribution of the experimental welded joint

study, the microhardness value was significantly influenced by the grain size and the microstructure (dislocation density and precipitate or intermetallic compound distribution). The

Fig. 10 TEM images showing second phases and dislocations in NZ of the welded joint at the traverse speed of 70 mm/min. **a** dislocation wall; **b** grain boundary and dislocations; **c** dislocations; **d** β-Mg$_{17}$Al$_{12}$ and dislocations; **e** SAED of β-Mg$_{17}$Al$_{12}$
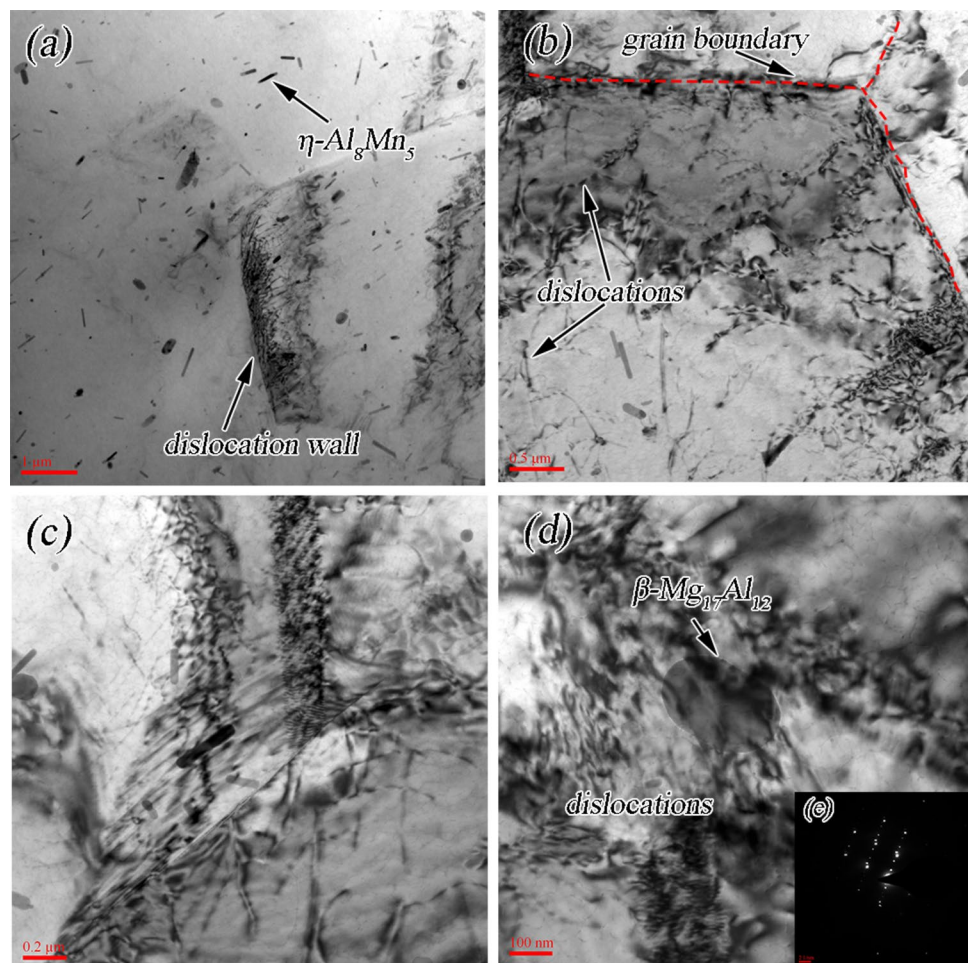
heterogeneous grain structures in different zones result from their different thermomechanical coupling behaviors.

The BM of AZ40M is not a precipitation-strengthened Mg alloy, and the microhardness variation is mainly caused by the grain size and dislocation density [29]. The dissolution and the reprecipitation of the second phase β-$Mg_{17}Al_{12}$ during FSW do not play an important role in the microhardness value. However, in the case of AZ61A, Al and Mg solid solutions and Al and Mg compounds play a substantial role in the microhardness value. In this study, the relatively large variation in the microhardness value of the experimental welded joints (NZ) with different traverse speeds is probably related to the dislocation density and residual stress evolution. Esparza et al. [30] reported that the slight change in the microhardness value in the NZ of an AZ31 alloy FSW welded joint is related to the high-density dislocations and residual stresses. During FSW, severe deformation occurs in the stir zone that causes high-density dislocations. The dislocation density increases with increasing traverse speed, and the microhardness value in the NZ increases gradually. However, in the welded joint when the traverse speed is 50 mm/min, the microhardness value is higher than that of the others because of the combined effect of the high-density dislocations and fine grain size. For the FSW Mg alloys, the basal slip hindered uneven grain boundaries, which also inhibited dislocation movement. In addition, the finer grains inhibit local plastic deformation because of the formation of many grain boundaries and consequently result in an increase in hardness [31]. In addition, because of the stirring effect in FSW, the alloy on the AS and RS underwent partial displacement; thus, the microhardness value in the (HAZ+TMAZ)-AS is higher than that of the BM-AS.

3.5 Tensile properties

The tensile properties of AZ40M/AZ61A dissimilar magnesium alloy joints obtained with different process parameters are shown in Fig. 12. When the traverse speed is 70 mm/min, the UTS and the YS achieve the maximum values of UTS (235 MPa) and YS (102 MPa), respectively. When the traverse speed is between 90 and 130 mm/min, the strength (YS and UTS) is similar. Therefore, the welded joint has obtained an exceptionally high strength value when the traverse speed is 70 mm/min. According to Table 2 and Fig. 12, yield stress (YS) and ultimate tensile strength (UTS) of the experimental welded joints are lower than those of the BMs. In general, the YS of the joint should be higher than that of the BMs due to the contribution of refined grains for DRX, while the results show the opposite fact. First, the strength is not strongly correlated to the hardness value because of the low hardness regions that exist in the welded joints. Second, the mechanical properties are also affected by the dislocation density and residual stresses. Third, textures play an important role in mechanical properties [32].

The YS and the UTS achieved a maximum when the traverse speed was 70 mm/min, which might be because of the effects of heat generation and plastic deformation during FSW. Hamilton et al. [33] reported that the YS is negatively related to temperature. In contrast, the higher traverse speed (larger than 90 mm/min) resulted in a lower heat input during FSW, which resulted in insufficient material flow in the NZ and caused the tensile properties to decrease. The elongation expressed similar results with the strength, and the elongations of all experimental welded joints were also relatively lower than that of BMs, as shown in Fig. 12b.
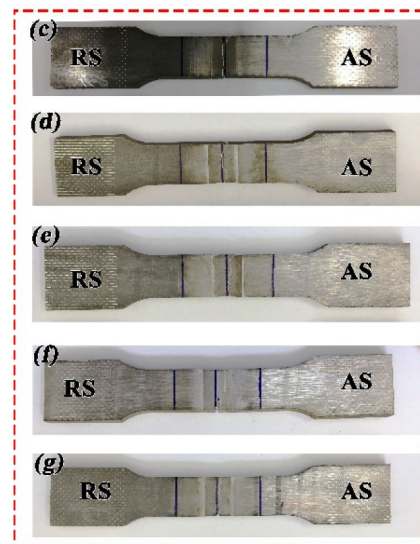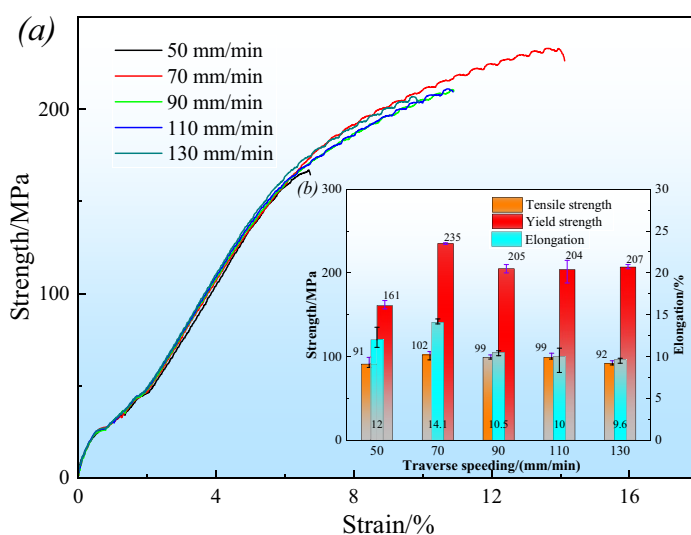

Fig. 12 The tensile properties of AZ40M/AZ61A dissimilar magnesium alloy joints

According to Fig. 12c-f, all experimental welded joints fractured in the center of the weld. Previous research on FSW joints of single Mg alloys reported similar fracture morphologies [23]. In summary, the traverse speed cannot significantly affect the tensile properties when the traverse speed is larger than 90 mm/min.

3.6 Fracture behavior

After the tensile test, the fracture morphology was studied by SEM and EDS to infer the fracture characteristics of the FSW joints, as shown in Fig. 13. Figure 13a shows the macroscopic fracture surface of the tensile specimen of the welded joint at a traverse speed of 50 mm/min. It can be observed that there is a loose structure caused by tunnel-type defects in the center of the thickness. Figure 13f-h is the fractographic of the top, middle, and bottom positions of the tensile fracture, all of which are composed of relatively flat cleavage planes, showing typical brittle fracture characteristics. Figure 13b-e shows the tensile fracture surfaces of the welded joints at traverse speeds from 70 mm/min to 130 mm/min. The tensile fracture surfaces consisted of brittle, ductile, and shear fracture features. The top surfaces show brittle fractography, as shown in Fig. 13k, n, q, t. The center-fractured surface shows the typical ductile feature, which consists of a number of dimples and tear ridges (Fig. 13j, m, p, s). The tear ridges are oriented along a certain direction and reveal some orientations. Yang et al. [34] proved that texture evolution can effectively affect the change in the direction of tear ridges. The bottom of welded joints at traverse speeds of 70 and 90 mm/min shows ductile fracture features with a number of dimples and tear ridges. Moreover, the bottom of the welded joints at traverse speeds of 110 and 130 mm/min exhibited brittle fracture features with a relatively flat and river morphology. The brittle fracture feature might be because of the higher traverse speed resulting in the lower heat input, which results in insufficient material flow in the NZ. The difference in fracture morphology in the plate thickness direction is also related to the heat input difference in the plate thickness direction of the FSW welded joint. The heat generated in the friction stir welding process is mainly generated by the friction between the rotating shoulder and the material to be welded. The top material of the welded joint is in direct contact with the shoulder surface, and the heat input and temperature obtained are higher than those at the center and bottom positions of the plate thickness. This difference in heat input in the thickness direction can lead to differences in the microstructure of the joint at different locations, which in turn affects the mechanical properties. In addition, Liu et al. [6] noted that second-phase particles play an important role in fracture.

The EDS analysis of the inclusions in the tensile fracture of the FSW joints obtained at traverse speeds of 70 and 130 mm/min is shown in Fig. 14. The SEM analysis shows that the inclusions are irregular block-like structures. These inclusions are mainly the second phase composed of Al, Mg, and Mn, which are inferred to be β-$Mg_{17}Al_{12}$ and η-Al_8Mn_5. These precipitated phase distributions play a strengthening role in the FSW joint. However, a high density of dislocations will form around the precipitated phase due to grain deformation and dislocation movement during the tensile process, resulting in stress concentration. This inhomogeneous stress state between the matrix and the precipitated phase leads to the aggregation of micropores and the formation of cracks, which eventually lead to the fracture of the joint [35].

4 Conclusions

Dissimilar friction stir welded AZ60M/AZ40A joints are achieved at different traverse speeds. The effects of traverse speed on joint formation, microstructure evolution, and mechanical properties are as follows:

(1) Sound dissimilar friction stir welded AZ60M/AZ40A joints with smooth surfaces were obtained at a wide range of traverse speeds of 70–130 mm/min. Surface liquefaction cracks and internal tunnel defects existed in the joint obtained at a traverse speed of 50 mm/min.

(2) As the traverse speed increases, the grain size of the NZ decreases. The microstructure of the NZ is mainly composed of fine recrystallized equiaxed grains. The second phase in the NZ is relatively fine and evenly distributed and is mainly the η-Al_8Mn_5 and β-$Mg_{17}Al_{12}$ phases. The combined effects of high-density dislocations and fine second phases promote mechanical properties.

(3) The strength increases as the traverse speed increases from 50 to 70 mm/min and then decreases as the traverse speed increases continually. An exceptionally high tensile strength of 235 MPa was achieved at a traverse speed of 70 mm/min.

(4) All tensile specimens fracture at the center of the welded joints, and the fracture surface shows typical ductile features.
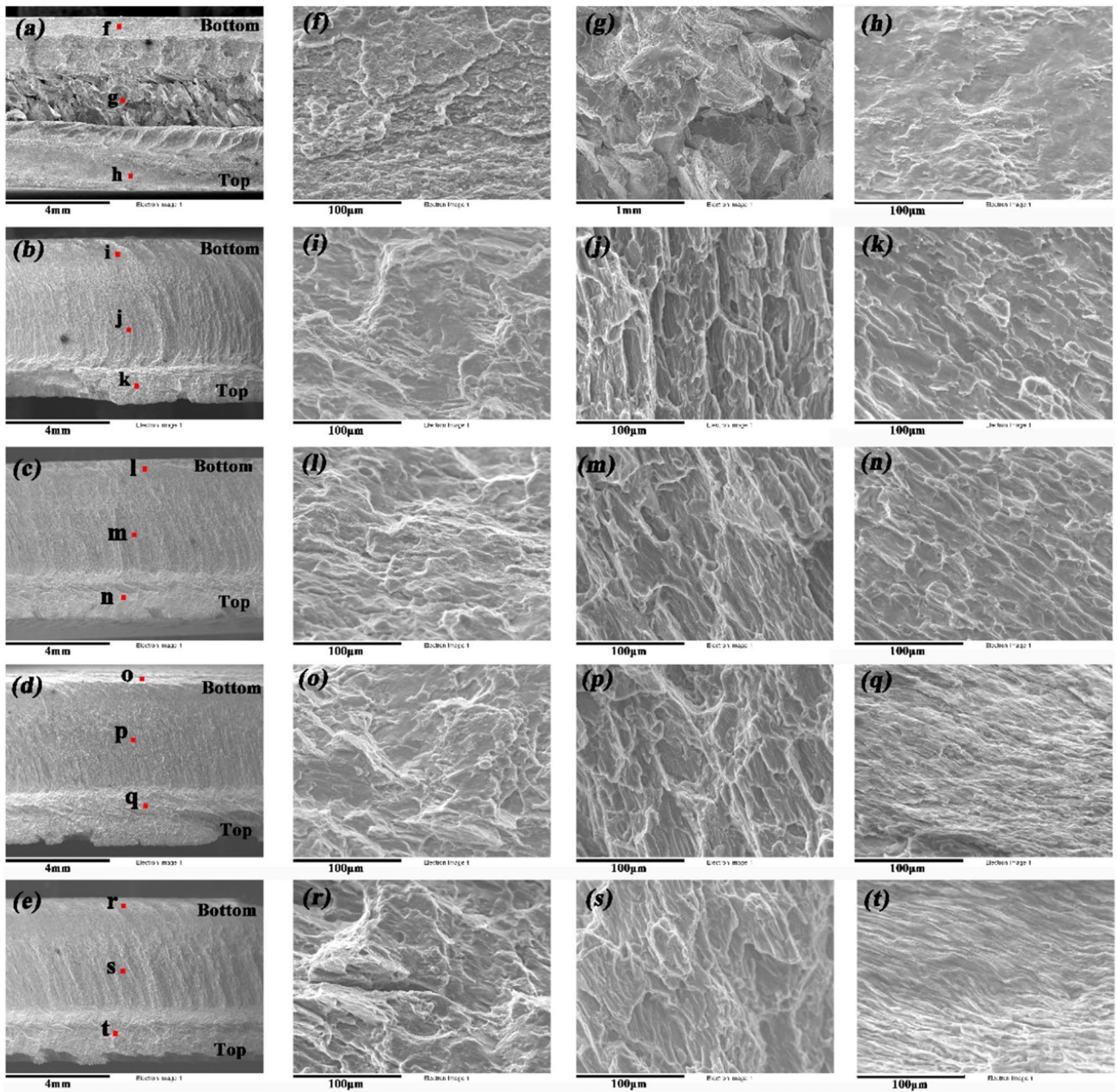
Fig. 13 Fractography of the fractured surfaces after tensile tests **a** 50 mm/min; **b** 70 mm/min; **c** 90 mm/min; **d** 110 mm/min and **e** 130 mm/min
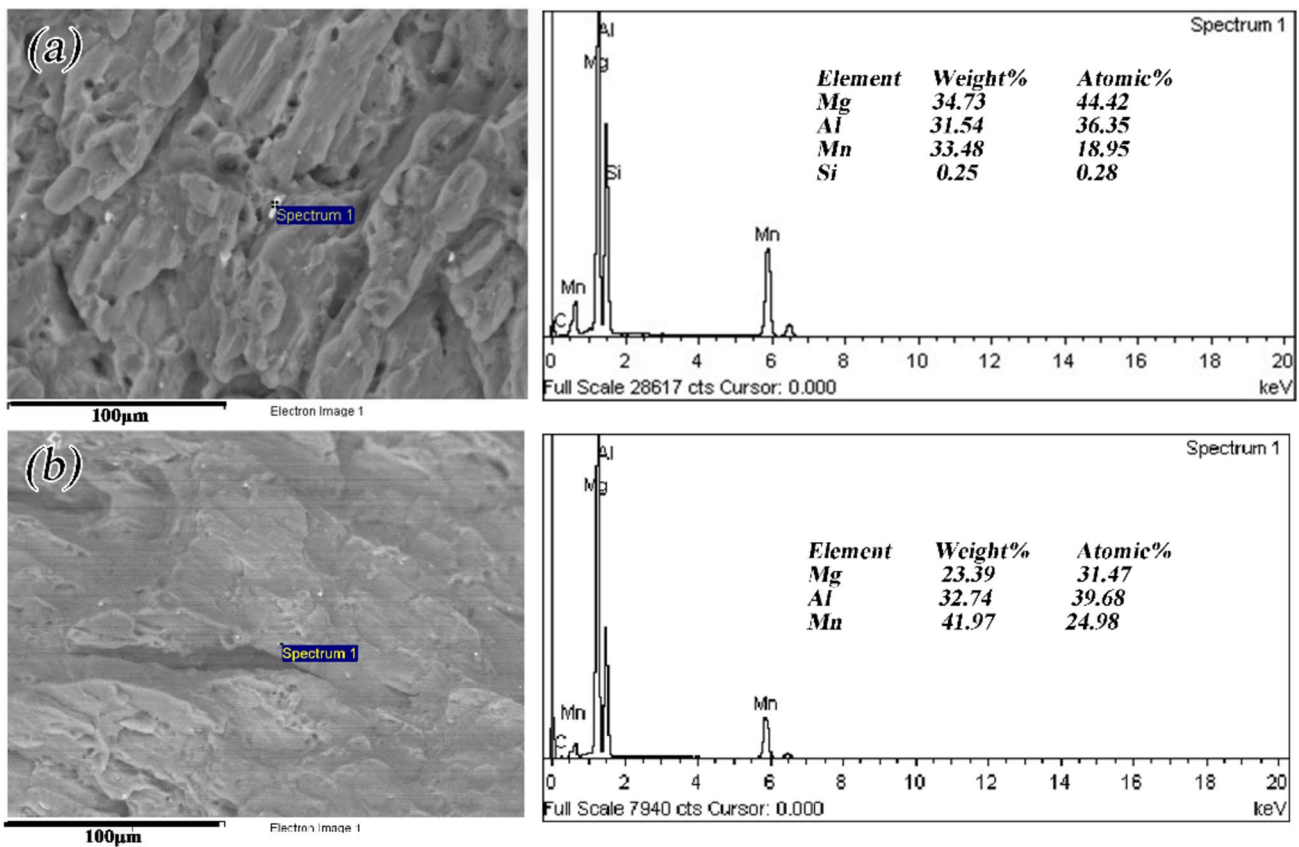
Fig. 14 EDS results of the inclusion phase **a** 70 mm/min; **b** 130 mm/min

Data and code availability All data generated or used during the study are included in the submitted article.

Declarations

Conflict of interest The authors declare that they have no conflict of interest.

Ethical approval Not applicable.

References

1. Mordike BL, Ebert T. Magnesium: properties—applications—potential. Mater Sci Eng A. 2001;302(1):37–45.
2. Nie JF. Precipitation and hardening in magnesium alloys. Metall Mater Trans A. 2012;43:3891–939.
3. Pan H, Ren Y, Fu H, Zhao H, Wang L, Meng X, Qin G. Recent developments in rare-earth free wrought magnesium alloys having high strength: a review. J Alloy Compd. 2016;663:321–31.
4. Singh K, Singh G, Singh H. Review on friction stir welding of magnesium alloys. J Magnes Alloys. 2018;6(4):399–416.
5. Li W, Niu PL, Yan SR, Patel V, Wen Q. Improving microstructural and tensile properties of AZ31B magnesium alloy joints by stationary shoulder friction stir welding. J Manuf Process. 2019;37:159–67.
6. Liu Z, Xin R, Wu X, Liu D, Liu Q. Improvement in the strength of friction-stir-welded ZK60 alloys via post-weld compression and aging treatment. Mater Sci Eng A. 2018;712:493–501.
7. Commin L, Dumont M, Masse JE, Barrallier L. Friction stir welding of AZ31 magnesium alloy rolled sheets: influence of processing parameters. Acta Mater. 2009;57(2):326–34.
8. Heidarzadeh A, Mironov S, Kaibyshev R, Çam G, Simar A, Gerlich A, Withers PJ. Friction stir welding/processing of metals and alloys: a comprehensive review on microstructural evolution. Prog Mater Sci. 2021;117:100752.
9. Wang W, Zhang W, Chen W, Yang J, Zhang L, Wang E. Homogeneity improvement of friction stir welded ZK61 alloy sheets in microstructure and mechanical properties by multi-pass lowered-temperature rolling. Mater Sci Eng A. 2017;703:17–26.
10. Zhang J, Liu H, Chen X, Zou Q, Huang G, Jiang B, Pan F. Deformation characterization, twinning behavior and mechanical properties of dissimilar friction-stir-welded AM60/AZ31 alloys joint during the three-point bending. Acta Metallurgica Sinica (English Letters). 2021;1–18.
11. Templeman Y, Hamu GB, Meshi L. Friction stir welded AM50 and AZ31 Mg alloys: microstructural evolution and improved corrosion resistance. Mater Charact. 2017;126:86–95.
12. He W, Zheng L, Xin R, Liu Q. Microstructure-based modeling of tensile deformation of a friction stir welded AZ31 Mg alloy. Mater Sci Eng A. 2017;687:63–72.
13. Luo XC, Kang LM, Liu HL, Li ZJ, Liu YF, Zhang DT, Chen DL. Enhancing mechanical properties of AZ61 magnesium alloy via

friction stir processing: effect of processing parameters. Mater Sci Eng A. 2020;797: 139945.

14. Yang J, Ni DR, Wang D, Xiao BL, Ma ZY. Friction stir welding of as-extruded Mg–Al–Zn alloy with higher Al content. Part I: formation of banded and line structures. Mater Charact. 2014;96:142–50.

15. Huang Y, Wang Y, Meng X, Wan L, Cao J, Zhou L, Feng J. Dynamic recrystallization and mechanical properties of friction stir processed Mg-Zn-Y-Zr alloys. J Mater Process Technol. 2017;249:331–8.

16. Lee CY, Lee WB, Yeon YM, Jung SB. Friction stir welding of dissimilar formed Mg alloys (AZ31/AZ91). Mater Sci Forum. 2005;486:249–52.

17. Liu D, Nishio H, Nakata K. Anisotropic property of material arrangement in friction stir welding of dissimilar Mg alloys. Mater Des. 2011;32(10):4818–24.

18. Sunil BR, Reddy GPK, Mounika ASN, Sree PN, Pinneswari PR, Ambica I, Amarnadh P. Joining of AZ31 and AZ91 Mg alloys by friction stir welding. J Magnes Alloys. 2015;3(4):330–4.

19. Liu D, Xin R, Zheng X, Zhou Z, Liu Q. Microstructure and mechanical properties of friction stir welded dissimilar Mg alloys of ZK60–AZ31. Mater Sci Eng A. 2013;561:419–26.

20. Luo C, Li X, Song D, Zhou N, Li Y, Qi W. Microstructure evolution and mechanical properties of friction stir welded dissimilar joints of Mg–Zn–Gd and Mg–Al–Zn alloys. Mater Sci Eng A. 2016;664:103–13.

21. Klenam DEP, Ogunwande GS, Omotosho T, Ozah B, Maledi NB, Hango SI, Bodunrin MO. Welding of magnesium and its alloys: an overview of methods and process parameters and their effects on mechanical behaviour and structural integrity of the welds. Manuf Rev. 2021;8:29.

22. Huetsch LL, Herzberg K, Dos Santos JF, Huber N. A study on local thermal and strain phenomena of high-speed friction stir-processed Mg AZ31. Weld World. 2013;57(4):515–21.

23. Shang Q, Ni DR, Xue P, Xiao BL, Ma ZY. Evolution of local texture and its effect on mechanical properties and fracture behavior of friction stir welded joint of extruded Mg-3Al-1Zn alloy. Mater Charact. 2017;128:14–22.

24. Xie L, Zhu X, Sun W, Jiang C, Wang P, Yang S, Song Y. Investigations on the material flow and the influence of the resulting texture on the tensile properties of dissimilar friction stir welded ZK60/Mg–Al–Sn–Zn joints. J Mater Res Technol. 2022;17:1716–30.

25. Zhang H, Wang HY, Wang JG, Rong J, Zha M, Wang C, Jiang QC. The synergy effect of fine and coarse grains on enhanced ductility of bimodal-structured Mg alloys. J Alloys Compds. 2019;780:312–7.

26. Lu S, Qi F, Chen J, Jia XD. Numerical simulation and experiment of temperature field on Mg alloy weld processed by friction-stir welding. J Comput Theor Nanosci. 2012;9(9):1231–5.

27. Zhou Z, Yue Y, Ji S, Li Z, Zhang L. Effect of rotating speed on joint morphology and lap shear properties of stationary shoulder friction stir lap welded 6061–T6 aluminum alloy. Int J Adv Manuf Technol. 2017;88:2135–41.

28. Guerra M, Schmidt C, McClure JC, Murr LE, Nunes AC. Flow patterns during friction stir welding. Mater Charact. 2002;49(2):95–101.

29. Kumar Singh U, Kumar Dubey A. Study of joining performance of dissimilar Mg alloys in friction stir welding. Proc Inst Mech Eng C J Mech Eng Sci. 2021;235(18):3554–62.

30. Esparza JA, Davis WC, Trillo EA, Murr LE. Friction-stir welding of magnesium alloy AZ31B. J Mater Sci Lett. 2002;21:917–20.

31. Afrin N, Chen DL, Cao X, Jahazi M. Microstructure and tensile properties of friction stir welded AZ31B magnesium alloy. Mater Sci Eng A. 2008;472(1–2):179–86.

32. Liu D, Xin R, Zhao L, Hu Y. Effect of textural variation and twinning activity on fracture behavior of friction stir welded AZ31 Mg alloy in bending tests. J Alloy Compd. 2017;693:808–15.

33. Hamilton C, Sommers A, Dymek S. A thermal model of friction stir welding applied to Sc-modified Al–Zn–Mg–Cu alloy extrusions. Int J Mach Tools Manuf. 2009;49(3–4):230–8.

34. Yang J, Xiao BL, Wang D, Ma ZY. Effects of heat input on tensile properties and fracture behavior of friction stir welded Mg–3Al–1Zn alloy. Mater Sci Eng A. 2010;527(3):708–14.

35. Suhuddin UFHR, Mironov S, Sato YS, Kokawa H, Lee CW. Grain structure evolution during friction-stir welding of AZ31 magnesium alloy. Acta Mater. 2009;57(18):5406–18.